Applied Catalysis B: Environmental 111–112 (2012) 445–455

Contents lists available at SciVerse ScienceDirect

Applied Catalysis B: Environmental

journal homepage: www.elsevier.com/locate/apcatb

Dual layer automotive ammonia oxidation catalysts: Experiments and computer simulation

A. Scheuer[a,b], W. Hauptmann[a], A. Drochner[b], J. Gieshoff[a], H. Vogel[b], M. Votsmeier[a,*]

[a] Umicore AG & Co. KG, Rodenbacher Chaussee 4, 63457 Hanau, Germany
[b] Ernst-Berl Institut, Technische Universität-Darmstadt, Petersenstr. 20, 64287 Darmstadt, Germany

ARTICLE INFO

Article history:
Received 12 July 2011
Received in revised form 18 October 2011
Accepted 21 October 2011
Available online 28 October 2011

Keywords:
Catalysis
Automotive
Dual layer
Ammonia oxidation
Platinum

ABSTRACT

Today, platinum based ammonia oxidation catalysts are applied in automotive exhaust systems to avoid ammonia slip from the SCR catalyst. In this paper we present a dual layer catalyst design with an additional SCR layer on top of the Pt/Al_2O_3 layer. Laboratory experiments show that the additional SCR layer significantly reduces NO formation, improves N_2 selectivity but also reduces the overall NH_3 conversion.

A mechanistically based kinetic model for NH_3 oxidation on platinum is presented. The model is parameterised using experiments with a single layer Pt/Al_2O_3 catalyst and well describes the NH_3 conversion and the selectivities for the products N_2, N_2O and NO. Additionally NO oxidation to NO_2 is included in the model.

Based on the mechanistic model for the platinum layer and a previously published model for the SCR layer, a 2-D model of the dual layer catalyst is set up. This model takes into account the diffusion and reaction in the two washcoat layers of one monolith channel. The 2-D model reproduces the experimental data well, with the mechanisms for the two layers parameterised in separate experiments and no additional parameters adjusted for the dual layer model.

Finally, the model is used to study the effect of some design parameters such as catalyst size, NO oxidation capacity of the Pt-layer and the thickness or diffusion coefficient of the SCR layer.

1. Introduction

One way to remove NO_x from automotive exhaust is through selective catalytic reduction (SCR) of NO_x with NH_3. In vehicle applications, NH_3 is generated on board by hydrolysing urea, which is carried in a separate tank as an aqueous solution. During operation of the SCR system, ammonia emissions into the environment need to be avoided. One way to solve this problem is through the application of an ammonia oxidation catalyst that is placed downstream of the SCR catalyst, either as a short zone on the same monolith or as a separate brick. Application of such an ammonia oxidation catalyst allows a more aggressive dosing of ammonia and, thus, can increase the NO conversion in the SCR system.

The purpose of this so-called ammonia slip catalyst is to oxidise ammonia to harmless nitrogen:

$$2NH_3 + 1.5O_2 \rightarrow N_2 + 3H_2O \quad (G1)$$

First-generation ammonia slip catalysts used platinum supported on an appropriate oxide. Unfortunately, ammonia oxidation on platinum is not selective for nitrogen. At higher temperatures, side reactions forming N_2O and NO_x in considerable amounts occur:

$$2NH_3 + 2O_2 \rightarrow N_2O + 3H_2O \quad (G2)$$

$$NH_3 + 1.5O_2 \rightarrow NO + 1.5H_2O \quad (G3)$$

$$NH_3 + 2O_2 \rightarrow NO_2 + 1.5H_2O \quad (G4)$$

More recently, ammonia slip catalysts with a dual layer architecture have been proposed [1]. These catalysts use a platinum-based oxidation catalyst in the lower layer and an SCR active catalyst in the upper layer. The idea behind this concept is that NO formed on the lower, platinum-containing layer can react with NH_3 in the upper SCR layer so that the overall output of NO is reduced and the selectivity for N_2 is increased (see Fig. 1).

Due to its importance for the production of nitric acid (Ostwald process), the oxidation of ammonia on Pt is an extremely well-studied reaction. The reaction has been investigated by a variety of experimental methods ranging from single crystal surface studies under ultra-high vacuum conditions to kinetic experiments under atmospheric pressure on polycrystalline catalyst samples. Furthermore, the energies of the reaction intermediates and the transition states have been computed using quantum mechanical methods. From these data, several micro-kinetics have emerged and are available in the literature [2–8]. Based on these reaction

* Corresponding author.
E-mail address: martin.votsmeier@eu.umicore.com (M. Votsmeier).

0926-3373/$ – see front matter © 2011 Elsevier B.V. All rights reserved.
doi:10.1016/j.apcatb.2011.10.032

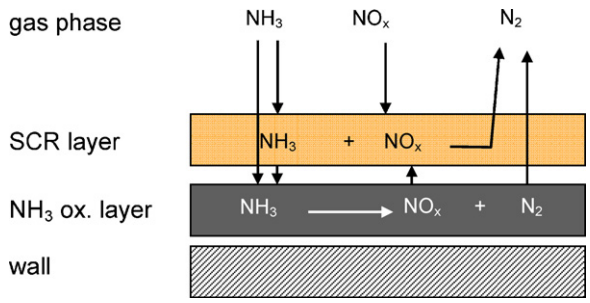

Fig. 1. Scheme of the dual layer catalyst concept.

mechanisms, we recently developed a mechanistic kinetic model that describes ammonia oxidation under automotive operating conditions [9].

Dual layer catalyst architectures are very common in automotive exhaust catalysis. One example is the three-way catalyst that today usually consists of a lower layer for the oxidation functionality and an upper layer for NO reduction on rhodium. A dual layer architecture has recently also been proposed for SCR catalysts [10]. Despite their practical importance, few publications on the simulation of such dual layer architectures exist. One recent exception is the work of Koltsakis et al. on catalysts that combine SCR and NO_x-adsorber functionalities in one layered system [11].

One likely reason for the lack of simulation studies on dual layer catalysts is the numerical effort associated with the simultaneous solution of the equations describing diffusion and reaction in the washcoat. We have recently shown that the simultaneous treatment of complex kinetics and washcoat diffusion is greatly facilitated by the use of mapped pre-computed rate data [12,13]. In this publication, we apply this rate mapping approach to construct a model of a dual layer ammonia oxidation catalyst.

Herein, we present a new kinetic model for platinum catalysed NH_3-oxidation and its parameterisation (Section 3.1). The new model is based on our previously published model [9] that is now extended to include the oxidation of NO to NO_2. Furthermore, we demonstrate that the new model as well as the SCR kinetics can be well represented by a rate mapping approach (Section 3.2). In Section 3.3, a 2-D model of a catalyst channel is presented. This model solves the transport and rate equations in the open channel and the two washcoat layers. The model performance is shown in Section 3.4, whereas in Section 3.5, the validated model is applied for sensitivity analysis while considering important design parameters such as the thickness of the upper layer, the diffusion coefficient of the upper layer and the length of the catalyst.

2. Methodology

2.1. Experimental

2.1.1. Catalyst samples

Three catalyst samples have been prepared for research purpose: one dual layer catalyst sample and two samples with corresponding single layer washcoats. Cordierite substrates with square channels, a cell density of 400 cpsi and a wall thickness of 6.5 mil were used for all catalyst samples. The ammonia oxidation layer consisted of a Pt/Al_2O_3 washcoat with a thickness of 10 μm (calculated for a circular shaped channel) and a Pt loading of 10 g ft^{-3}. The SCR layer was a Fe–zeolite system with a washcoat thickness of 71 μm (calculated for a circular shaped channel). All catalysts have been aged hydrothermally for 16 h at 700 °C.

2.1.2. Experimental setup

All experiments were performed in a tubular quartz reactor. Samples were measured as drill cores with a 1 in. diameter and 3/4 in. length. To monitor the thermal behaviour of the samples, 4 thermocouples were placed inside the monolith. Temperature deviations of the thermocouples without any reaction at typical experimental conditions were smaller than 3 K. The deviations are in the same range as the uncertainty of the thermocouples and the calculated adiabatic temperature rise of the oxidation of 300 ppm NH_3 (2.5 K) under the given conditions.

The composition of the gas phase was monitored online with an FT-IR spectrometer.

2.1.3. Light-off/light-down experiments

Before the light-off/light-down experiments, the samples were pre-treated with the reaction gas mixture at 500 °C for 1 h. After cooling to 150 °C, the light-off temperature ramp was performed at a heating rate of 2 K min^{-1} up to 500 °C. Subsequently, the light-down ramp was applied down to 150 °C at the same rate. The feed gas composition was held constant during the experiment. Reproducibility was assured for the Pt single layer catalyst by performing an additional light-off/light-down ramp after the first one. Due to the slow heating/cooling ramp, axial temperature gradients in the monolith were negligible.

2.1.4. Steady-state experiments

The steady-state experiments began with a pre-treatment under NO and O_2 at 500 °C for 1 h. Thereafter, the catalyst was cooled under a N_2 atmosphere to the test temperature. A concentration program was applied at a constant temperature. Each concentration point was held until no significant signal change could be observed.

2.2. Simulation

2.2.1. Surface rate equations

Ammonia oxidation on platinum is described by a mechanistic kinetic model. The reaction rates r_j for the individual reactions j are calculated by the following formula:

$$r_j = \Gamma k_{0j} \exp\left(-\frac{E_{aj}}{RT}\right) \prod_i \theta_i^{|\nu_{ij}|} \prod_i c_i^{|\nu_{ij}|} \quad (1)$$

where Γ is the concentration of surface sites, k_{0j} and E_{aj} are the pre-exponential factor and the activation energy of reaction j, respectively, θ_i is the surface coverage of surface species i, c_i is the concentration of the gas species i and ν_{ij} is the stoichiometric coefficient of species i in reaction j.

For each species i, a source term $\dot{s}_i$ is computed from the rates for the individual reactions:

$$\dot{s}_i = \sum_j \nu_{ij} r_j \quad (2)$$

2.2.2. Kinetic model of the SCR layer

The kinetics of the SCR catalyst have been extensively studied in the literature, and a number of kinetic models have been published [14–21]. The kinetic model used in this work was previously published in [18] and [16].

The model takes into account the following reactions:

NH_3 adsorption/desorption:

$$NH_3 + \theta^* \leftrightarrow NH_{3,ad} \quad (R_{SCR}1)$$

NH_3 and NO oxidation:

$$2NH_3 + 1.5O_2 \rightarrow N_2 + 3H_2O \quad (R_{SCR}2)$$

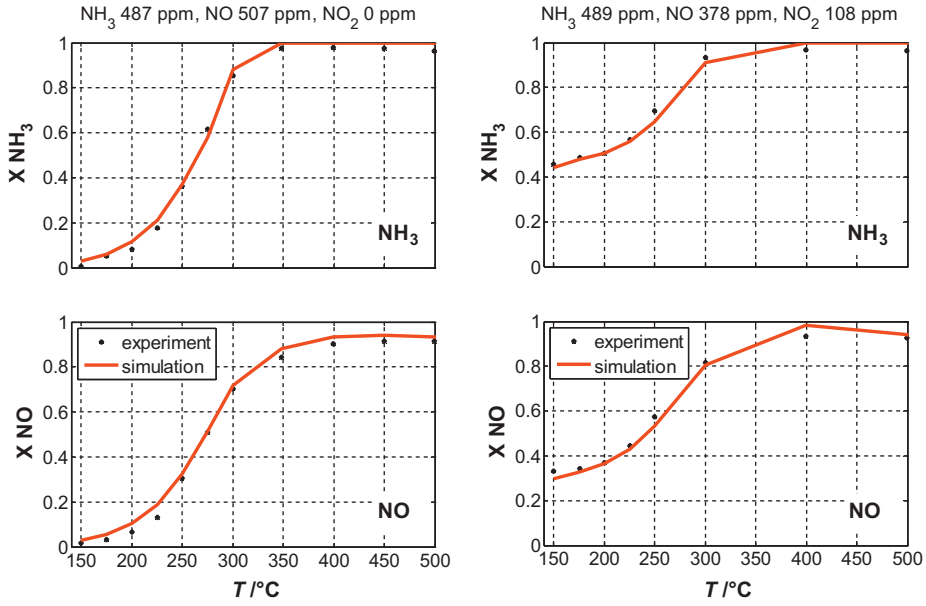

Fig. 2. Quality of the SCR layer mechanism: steady-state conversion of NH_3 and NO are shown for a feed gas for the standard SCR reaction and for a feed gas containing 25% NO_2 in NO_x. The simulation results were compared with the experimental data (O_2: 5%, SV: 50,000 h^{-1}).

$$NO + 0.5O_2 \rightarrow NO_2 \quad (R_{SCR}3)$$

The SCR reaction with NO, NO/NO_2 and NO_2:

$$4NH_3 + 4NO + O_2 \rightarrow 4N_2 + 6H_2O \quad (R_{SCR}4)$$

$$2NH_3 + NO + NO_2 \rightarrow 2N_2 + 3H_2O \quad (R_{SCR}5)$$

$$8NH_3 + 6NO_2 \rightarrow 7N_2 + 12H_2O \quad (R_{SCR}6)$$

The rate equations and kinetic parameters are reported in [18]. In [18], it was experimentally observed that the rate of NH_3 oxidation increased in the presence of NO/NO_2. This increase was taken into account in an empirical approach with a variable stoichiometric factor for the NH_3 consumption in reactions ($R_{SCR}4$) and ($R_{SCR}6$). Technically, the temperature-dependence of the stoichiometry factors was implemented by increasing the rate of NH_3 oxidation ($R_{SCR}2$) under conditions where ($R_{SCR}4$) or ($R_{SCR}6$) takes place:

$$r_2 = r_2^0 + f_1(T) \times r_4 + f_2(T) \times r_6 \quad (3)$$

where r_2^0 is the rate of ammonia oxidation in the absence of NO and NO_2 and $f_1(T)$ and $f_2(T)$ are temperature dependent look-up tables. A similar approach has recently also been presented by Colombo et al. [22].

The model was parameterised using a large amount of experimental data (see [18] for details). In the context of the current work, the model's ability to describe the steady state reaction of NH_3 with NO_x (including smaller concentrations of NO_2) was of particular importance. Fig. 2 demonstrates the performance of the model under these conditions.

2.2.3. 1-D reactor model

A 1-D model of a single monolith channel was used for adaptation of the kinetic models to the experimental data (Section 3.1). The monolith was discretised in a number of axial volume elements, and the heat and mass balances were solved for each volume element. These balances accounted for convection, gas-wall heat and mass transfer and the reactions in the wall. A more detailed description of the simulator can be found in [23].

2.2.4. Efficient implementation of the source terms by a spline mapping approach

A spline mapping approach was used for efficient implementation of the kinetic models in the 2-D model of the dual layer catalyst. In a pre-processing step, a large number of steady state source terms were computed for different gas concentrations and temperatures. From these data, a spline function was constructed that was used for computation of the source terms during the runtime of the 2-D simulator.

2.2.4.1. Computation of steady state source terms. Steady state surface concentrations for a specific gas composition and surface temperature were obtained by numerically integrating the ordinary differential equation

$$\frac{d\theta_i}{dt} = \frac{\dot{s}_i}{\Gamma} \quad (4)$$

for the surface species until a steady state was reached. During this integration, the gas concentrations and temperature remain constant. The integration was performed using the numerical solver DASSL [24].

2.2.4.2. Construction and evaluation of the spline functions. Steady state source terms were computed for input data located on a rectangular grid, and the toolbox of de Boor [25] was used to construct a multivariate tensor spline interpolation function. The source term s_i of species i is a function of the scaled independent variables $\ln(y_{NH_3})$, $\ln(y_{NO})$, $\ln(y_{NO_2})$ and $1/T$, where y is the mole fraction of the corresponding gas species. Source terms for species that appear only as products (N_2O, N_2) or appear only as educts (NH_3) are mapped as their logarithms $\ln(s_i)$. This logarithmic scaling is not possible for source terms that assume positive and negative values (NO, NO_2) [13]. All spline interpolation functions used in this work were of the polynomial order of two. During the runtime of the 2-D simulator, the spline functions were evaluated using the Fortran subroutine presented in [26].

2.2.4.3. Performance measure of the rate mapping. To determine the accuracy of the spline interpolation functions to benchmark the quality of the spline interpolation, test sets were computed that

consisted of 10,000 data points randomly sampled from the input space of the mapping. A mixed absolute/relative error was computed according to:

$$e_n = \frac{\dot{s}_{\mathrm{spline},n} - \dot{s}_{\mathrm{dassl},n}}{\max(\dot{s}_{\mathrm{dassl},n}, \dot{s}_{\mathrm{threshold},n})} \quad (5)$$

where $\dot{s}_{\mathrm{spline},n}$ is the source term of data point n obtained by the spline interpolation and $\dot{s}_{\mathrm{dassl},n}$ is the source term calculated with the numerical solver. For source terms with a value above a threshold value $\dot{s}_{\mathrm{threshold},n}$ Eq. (5) computes a relative error. For values below $\dot{s}_{\mathrm{threshold},n}$, a scaled absolute error is computed. For each data point, the threshold value $\dot{s}_{\mathrm{threshold},n}$ is computed as $\dot{s}_{\mathrm{threshold},n} = c_i/\tau_{\mathrm{Ref}}$, where c_i is the gas phase concentration of the species i. τ_{Ref} is a typical residence time for a reactor simulation. A value of 12 ms is used for τ_{Ref} at standard conditions, which is the upper limit of the residence times for the simulations presented in Section 3.3. For those species that do not appear as input parameters for the mapping (N_2, N_2O), a value of c_i = 50 ppm was used for all points of the data set.

From the errors for the individual points of the data set, an average error was computed according to:

$$\hat{e} = \frac{1}{N}\sqrt{\sum_{n}^{N}(e_n^2)}, \quad (6)$$

where N is the number of data points in the test set.

A more detailed description of the procedure and a motivation for the use of this relatively complex error measure are provided in [13] and [26].

2.2.5. 2-D reactor model

The 2-D model of one individual monolith channel solved the transport and reaction equations for the two washcoat layers and the open channel. The model was similar to the model used in [13]. The main difference was that, here, the reaction diffusion equation was solved for two washcoat layers.

To reduce the complexity of the model, the quadratic shape of the channel and the fillet shape of the washcoat [27] were neglected so that the channel could be approximated as a rotational symmetric channel. The resulting geometry of the model is shown in Fig. 4.

The mass balance for convection and diffusion in the gas phase of the open channel is:

$$\nabla \cdot (-D_i \nabla c_i + c_i u) = \frac{\partial c_i}{\partial t} \quad (7)$$

where u is the axial velocity given by a parabolic flow profile. The gas phase diffusion coefficients of the individual species D_i were computed according to Fuller [28].

The balance equation for reaction and diffusion in the two washcoat layers is:

$$\nabla \cdot (-D_{eff} \nabla c_i) = \dot{s}_i \quad (8)$$

The source terms $\dot{s}_i$ were computed by evaluating the spline interpolation functions.

The effective diffusion coefficients D_{eff} for the washcoat were computed based on the gas phase diffusion coefficients according to:

$$D_{eff} = \frac{\varepsilon}{\tau} D_{gas} \quad (9)$$

Values for the porosity ε and the tortuosity factor τ were taken from the theoretical work of Kočí for porous alumina [29]. Using these factors, a value of $3.75 \times 10^{-6}\,m^{-2}\,s$ for the diffusion coefficient of NO at 200 °C was obtained. This value is in good agreement with the value of $\sim 3.0 \times 10^{-6}\,m^{-2}\,s$ used by Nova et al. [30] for the description of internal diffusion limitations in a zeolite-based SCR catalyst. The value is also in reasonable agreement with the effective diffusion coefficients measured by Zhang et al. for an alumina washcoat [31].

The 2-D model of the monolith channel was implemented in the commercial simulation package Comsol Multiphysics, Version 3.3a.

In this paper, only an isothermal model is solved. This is justified by the fact that the adiabatic temperature rise for the combustion of 300 ppm NH_3 is less than 2.5 K. Additional implementation of the heat balance in Comsol would be straightforward.

Table 1
Reaction mechanism for the platinum catalyst. Pt-h and Pt-t are two different active sites.

Reaction			This work[a]
$NH_3 + Pt\text{-}t \rightarrow Pt\text{-}t\text{–}NH_3$	(R1)	k_0	1.9×10^1
		E_a	0
$Pt\text{-}t\text{–}NH_3 \rightarrow NH_3 + Pt\text{-}t$	(R2)	k_0	6.6×10^4
		E_a	116
$O_2 + 2Pt\text{-}h \rightarrow 2Pt\text{-}h\text{–}O$	(R3)	k_0	2.6×10^2
		E_a	0
$2Pt\text{-}h\text{–}O \rightarrow O_2 + 2Pt\text{-}h$	(R4)	k_0	1.2×10^{12}
		E_a	128
$Pt\text{-}t\text{–}NH_3 + 1.5Pt\text{-}h\text{–}O \rightarrow$ $Pt\text{-}h\text{–}N + 1.5H_2O + 0.5Pt\text{-}h + Pt\text{-}t$	(R5)	k_0	2.8×10^{16}
		E_a	139
$Pt\text{-}h\text{–}NO \rightarrow NO + Pt\text{-}h$	(R6)	k_0	6.0×10^{17}
		E_a	126
$NO + Pt\text{-}h \rightarrow Pt\text{-}h\text{–}NO$	(R7)	k_0	2.9×10^2
		E_a	0
$2Pt\text{-}h\text{–}N \rightarrow N_2 + 2Pt\text{-}h$	(R8)	k_0	1.2×10^{19}
		E_a	181
$Pt\text{-}h\text{–}N + Pt\text{-}h\text{–}O \rightarrow Pt\text{-}h\text{–}NO + Pt\text{-}h$	(R9)	k_0	2.8×10^{13}
		E_a	126
$Pt\text{-}h\text{–}NO + Pt\text{-}h\text{–}N \rightarrow N_2O + Pt\text{-}h$	(R10)	K_0	1.0×10^{20}
		E_a	139
$Pt\text{-}h\text{–}NO + Pt\text{-}h\text{–}O \rightarrow Pt\text{-}h\text{–}NO_2 + Pt\text{-}h$	(R11)	k_0	6.8×10^{14}
		E_a	115
$Pt\text{-}h\text{–}NO_2 + Pt\text{-}h \rightarrow Pt\text{-}h\text{–}NO + Pt\text{-}h\text{–}O$	(R12)	k_0	3.2×10^{11}
		E_a	83
$Pt\text{-}h\text{–}NO_2 \rightarrow NO_2 + Pt\text{-}h$	(R13)	k_0	1.3×10^{14}
		E_a	100
$NO_2 + Pt\text{-}h \rightarrow Pt\text{-}h\text{–}NO_2$	(R14)	k_0	4.8×10^4
		E_a	0

[a] E_a is reported in kJ mol^{-1}, k_0 for (R1), (R3), (R7) and (R14) is in m^3 s^{-1} mol^{-1} K^{-1} and the rest are in s^{-1}.

3. Results and discussion

3.1. NH_3-oxidation mechanism on Pt

3.1.1. Model development

The kinetic model used in this work is based on our previously published model for NH_3 oxidation on platinum under automotive operating conditions [9]. It has been shown that this model accurately reproduces the ammonia conversion and the selectivity for N_2, N_2O and NO. Furthermore, the model takes into account the SCR reaction of NO with NH_3 and reproduces the associated increase in N_2O selectivity when NO is present in the feed.

In this work, the model was extended by additional surface reactions to take into account the oxidation of NO to NO_2, which is experimentally observed above 300 °C but was neglected by our previous model. In the current study, where the Pt catalyst is combined with an SCR layer, NO_2 formation may be of importance

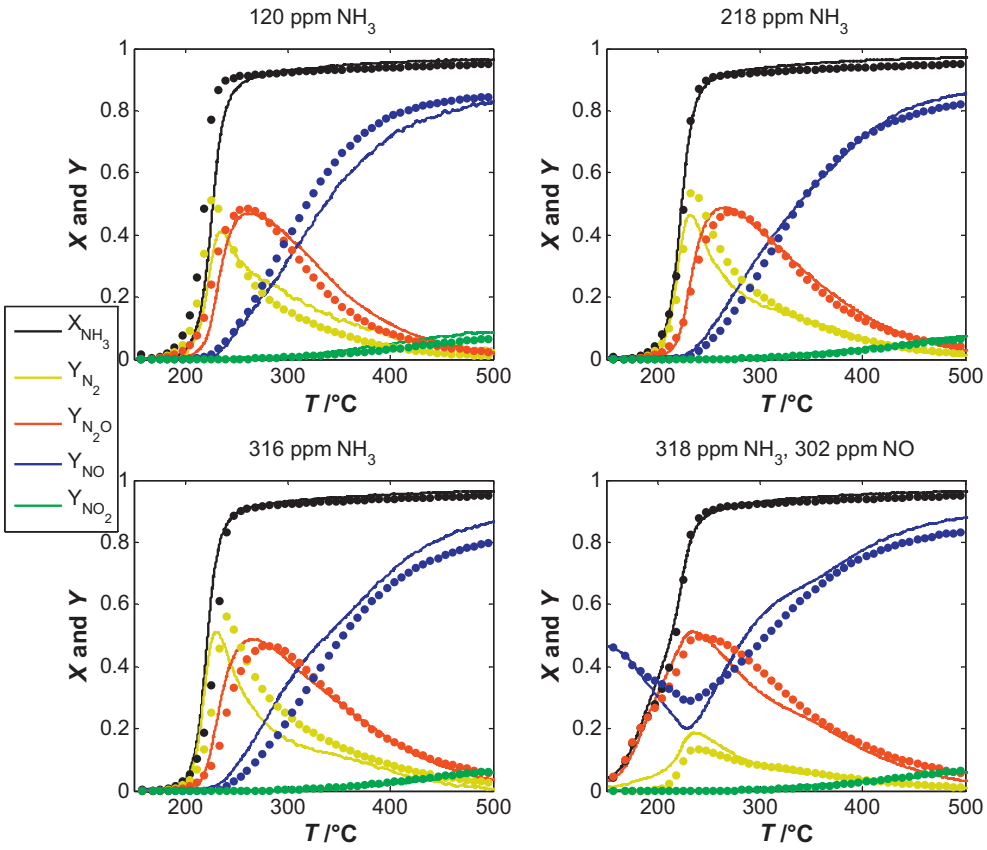

Fig. 3. Quality of the NH_3-oxidation layer mechanism: conversion and yield of gas species vs. temperature for four different feed compositions. The experiment had an upward temperature ramp at a heating rate of 2 K min^{-1}, 6% O_2, 5% H_2O and a space velocity of 300,000 h^{-1}.

because NO_2 can potentially increase the conversion of NO and NH_3 in the upper layer (the so-called fast SCR reaction ($R_{SCR}5$)).

The surface reactions included in the kinetic model are listed in Table 1. Reactions (R1)–(R10) were taken from our previous model [9]. Reactions (R11)–(R14) were added to describe the oxidation of NO to NO_2. These reactions were taken from [32].

The model was parameterised by simultaneously fitting data from several experiments under different inlet conditions. Initial values for the parameters of reactions (R1)–(R10) were taken from [9], while those of reactions (R11)–(R14) were from [32]. Fig. 3 shows the experimental data and simulation results for the parameterised mechanism. Obviously, the model was able to reproduce the behaviour of the catalyst well over a wide range of operating conditions. For the parameterisation of the kinetic model it was assumed that the observed kinetics is not influenced by internal mass transfer limitations. This assumption is justified by the low washcoat loading of the monolith. In a previously published study [13] that used the same catalyst as used in this paper we showed that at washcoat loadings below 25 g L^{-1} the effect of internal diffusion limitations can be neglected.

To ensure thermodynamic consistency of the NO oxidation submodel, only the parameters of the forward reaction of the reaction of Pt-h–O with Pt-h–NO (R11) were included in the parameter optimisation, while the rate of the reverse reaction was determined in such a way that the entire reaction sequence for NO oxidation (reactions (R11)–(R14)) fulfilled the thermodynamic equilibrium requirements [33]. Note that the calculation of the reaction rates for the forward and reverse reactions by Eq. (1) implies temperature-independent reaction enthalpies and entropies. For this reason, a kinetic model of this form naturally ignores the temperature dependency of these thermodynamic quantities. In this work, values for the reaction enthalpy and entropy at 600 K were used.

In experiments with subsequent heating and cooling phases, NH_3 oxidation showed a hysteresis behaviour with higher NH_3 conversion during the cool down phase. The corresponding experimental data are presented in [9]. In the current work, we focused on the heating behaviour of the catalyst, so all data used for parameterisation of the mechanism and shown in Fig. 3 were recorded during a heating ramp.

3.1.2. *Mechanistic surface kinetics versus empirical global models*

There is a long lasting debate over the usefulness of detailed mechanistic models for practical simulation work. The standard argument in favour of detailed chemical models is that these models may allow a better extrapolation to operating conditions not considered during construction of the model [34]. One standard argument against mechanistic models is the large number of parameters involved in them.

The mechanistic model of Table 1 contains 22 free kinetic parameters, if thermodynamic constraints are taken into account. Table 2 lists all global reactions that are represented by the surface reaction mechanism in Table 1. A kinetic model based on global

Table 2
The global reactions represented by the mechanistic model for NH_3 oxidation on Pt in Table 1.

Global reactions	
$2NH_3 + 1.5O_2 \rightarrow N_2 + 3H_2O$	(G1)
$2NH_3 + 2O_2 \rightarrow N_2O + 3H_2O$	(G2)
$NH_3 + 1.5O_2 \rightarrow NO + 1.5H_2O$	(G3)
$NH_3 + 2O_2 \rightarrow NO_2 + 1.5H_2O$	(G4)
$2NH_3 + 2NO + 1.5O_2 \rightarrow 2N_2O + 3H_2O$	(G5)
$NO + 0.5O_2 \leftrightarrow NO_2$	(G6)
$2NH_3 + 2NO_2 + 0.5O_2 \rightarrow 2N_2O + 3H_2O$	(G7)

Table 3
Input range for the mapping.

	Pt mechanism			SCR mechanism		
	lb	ub	Points	lb	ub	Points
T (°C)	150	500	20	150	500	20
X_{NH_3} (mol mol^{-1})	1×10^{-8}	1×10^{-3}	20	1×10^{-8}	1×10^{-3}	20
X_{NO} (mol mol^{-1})	1×10^{-8}	1×10^{-3}	20	1×10^{-8}	1×10^{-3}	20
X_{NO_2} (mol mol^{-1})	1×10^{-8}	3×10^{-4}	20	1×10^{-10}	1×10^{-3}	20

lb, lower boundary; ub, upper boundary.

reactions would consist of 7 reactions. At least 14 kinetic parameters would be required if each reaction is described by only a pre-exponential factor and an activation energy. Furthermore, the global model will require some additional parameters, such as reaction orders or inhibition terms that describe the dependency of the individual rates on the concentrations. If one assumes only 2 such additional parameters per reaction, then the result is 28 rate parameters, 6 more than the 22 parameters of the mechanistic model. This example shows that for relatively dense reaction networks where each surface reaction contributes to several global reactions, mechanistic kinetic models do not necessarily contain more parameters than comparable empirical global models. However, mechanistic models do many seemingly simple things automatically right that need to be explicitly considered during the development of a global rate model. Some examples are the competition of different species for the same surface site, the interaction of competing elementary reactions and the fact that no species can be consumed faster than the collision frequency with the catalyst surface.

3.2. Efficient implementation of the source terms by a spline mapping approach

In this paper, the ammonia oxidation kinetics in the lower layer and the SCR kinetics in the upper layer were implemented in the reactor model using a rate mapping approach. This means that during the solution of the reactor model for each mesh point in the washcoat the local source term (Eq. (8)) is computed by interpolation of a spline map. For each of the two layers, a spline function was constructed that interpolated the source terms as a function of temperature and the input concentrations of NH_3, NO and NO_2. The ranges for each of the four input parameters are listed in Table 3. Twenty data points were used for each input dimension, which resulted in a data set with 160,000 data points. All source terms were computed for a constant oxygen concentration of 6%, which was justified by the large excess of oxygen in the reaction mixture.

To characterise the performance of the spline maps, test data sets were created by sampling 10,000 data points randomly from the respective input spaces. In Table 4, the average errors $\hat{e}$ are listed for both mechanisms.

All calculations were performed on a Pentium 4 3.0 GHz Processor with 2.5 GB RAM. A comparison of the calculation times of the numerical solver and the spline approximation is shown in Table 5.

One numerical solution of the 2-D model requires 33,800,000 calls to the spline interpolation routine. Application of the mapping approach speeds up the solution of the 2-D model by a factor of 27 compared to a numerical solution of rate equations [35].

Table 4
Accuracy of the spline map against a test set of 10,000 random points.

	Pt mechanism		SCR mechanism	
	Mapped quantity	$\hat{e}$	Mapped quantity	$\hat{e}$
NH_3	$\ln(-\dot{s})$	3.7×10^{-3}	$\ln(-\dot{s})$	2.5×10^{-3}
N_2	$\ln(\dot{s})$	5.1×10^{-3}	$\ln(\dot{s})$	2.4×10^{-3}
N_2O	$\ln(\dot{s})$	4.0×10^{-3}	–	–
NO	$\dot{s}$	6.0×10^{-3}	$\dot{s}$	6.7×10^{-3}
NO_2	$\dot{s}$	3.6×10^{-3}	$\dot{s}$	6.3×10^{-3}

3.3. 2-D simulation

Using the mapped rate data discussed in Section 3.2, a 2-D model of one monolith channel was set up in the commercial simulation package Comsol (see Section 2.2.5). The model solved the coupled transport and reaction equations in the gas phase and in the two washcoat layers. Fig. 4 shows typical concentration profiles of NH_3 and NO obtained by this simulation. High NO concentrations were observed in the platinum layer, but little of the NO formed in this layer reached the gas phase. This result showed that a catalyst with dual layer architecture should indeed be effective in reducing NO emissions from NH_3 oxidation. For NH_3, a strong gradient was observed in the upper SCR layer, which indicated that the SCR layer acted as a diffusion barrier for the oxidation of ammonia on the platinum layer. Such a diffusion limitation will lead to a reduced NH_3 conversion for the dual layer catalyst compared to the catalyst with only a single platinum layer.

Fig. 5 (right side) compares the simulated output concentrations for the dual layer catalyst and a platinum-only single layer catalyst, both with identical assumed platinum loadings. One obvious result is that the additional SCR layer reduces the overall NH_3 conversion. This result can be explained by the diffusion resistance (compare Fig. 4) of the SCR layer, which leads to lower NH_3 concentrations and hence lower NH_3 conversion rates in the platinum layer. Another conclusion from Fig. 5 is that the additional SCR layer indeed should reduce NO emissions and enhance selectivity for N_2. The increased NO conversion is explained by the reaction of NO and counter diffusing NH_3 in the SCR layer.

3.4. Comparison with experimental data

Fig. 5 presents experimental results for a dual layer catalyst and a single layer catalyst. As predicted by the model, the dual layer catalyst showed a significantly reduced NH_3 conversion compared to a single layer catalyst with an identical platinum layer. This result is explained by the diffusion limitation in the upper layer. It should be noted that the data in Fig. 5 were measured at an extremely high space velocity of 300,000 h^{-1}. At 300 °C, this corresponds to a residence time of only 5.7 min. Furthermore, the catalyst used for the experiments had a relatively high loading of SCR washcoat. In Section 3.5.1, we show that for a given space velocity, reducing the loading of the SCR catalyst increases the NH_3 conversion. In Section

Table 5
Comparison of the calculation times for the computation of 10,000 data points with the numerical solver and spline approximation. The computation times reported for the spline mapping include several calls of the interpolation routine (one call for each gas species).

Model	Dassl (s)	Spline (s)	Speed-up
Pt	97.5	1.5	65.0
SCR	29.5	1.2	24.6

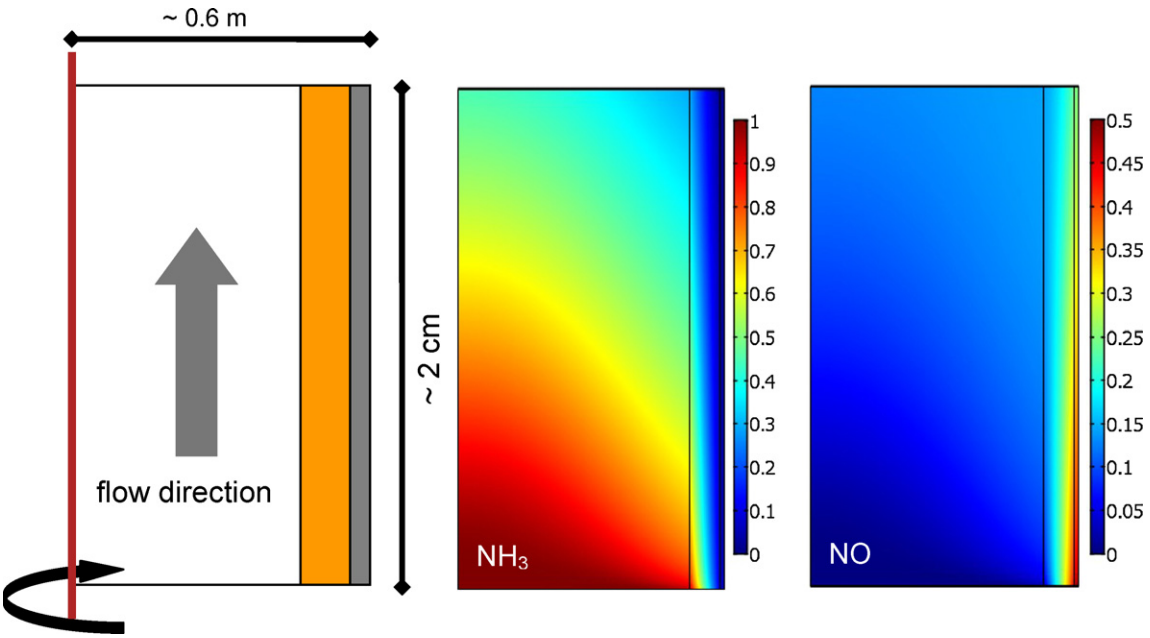

Fig. 4. Spatially resolved profiles of the relative concentrations of NH_3 and NO divided by the NH_3 input concentration for the 2-D model of the dual layer catalyst (300 ppm NH_3, 6% O_2, GHSV 300,000 h^{-1}, 400 °C). On the left side, a scheme of the model geometry is shown. The vertical red line represents the symmetry axis, the white area the gas phase, the orange area the SCR washcoat and the grey area the Pt washcoat. (For interpretation of the references to color in this figure legend, the reader is referred to the web version of this article.)

3.5.3 it is shown, that the NH_3 conversion also increases at lower gas velocities.

Overall, the experimental data (conversion and product selectivities) for the dual layer catalyst were surprisingly well reproduced by the model, especially if one takes into account that the kinetic parameters for the individual layers were obtained from separate experiments with single layer catalysts and no additional parameters were adapted for the dual layer model.

3.5. Numerical study of design parameters for the dual layer catalyst

The development of a dual layer catalyst requires optimisation of the catalyst formulation as well as the washcoat loading for both catalyst layers. Naturally, this leads to a larger number of design parameters compared to a single layer catalyst. In the following, the numerical model is used to study the effect of a few important design parameters.

3.5.1. Variation of the SCR washcoat loading

In this section, we study the effect of a variation in the washcoat loading, which is equivalent to a variation in washcoat thickness (assuming a constant density of active sites). Fig. 6 compares simulation results for different washcoat loadings. The NH_3 conversion decreased nearly linearly with increasing washcoat thickness. However, the selectivity for N_2 increased with increasing thickness of the SCR layer.

As a consequence, there is a natural trade-off between lowering the conversion of ammonia and increasing the selectivity for nitrogen. This trade-off indicates that the optimal thickness will depend on the specific vehicle application and relative importance of NH_3 conversion and product selectivity in the particular development project.

3.5.2. Variation of the diffusion coefficient in the SCR layer

The results presented in the previous sections indicated that the SCR layer in the dual layer catalyst acts as a diffusion barrier for NH_3, and in this way, limits the NH_3 conversion that can be obtained with the catalyst. The obvious importance of the diffusion in the SCR layer strongly implicates the layer's diffusion coefficient as an additional design parameter.

Fig. 7 presents simulation results using different diffusion coefficients. As expected, higher diffusivities lead to higher NH_3 conversions. Surprisingly, variation of the diffusion coefficients had little effect on the product selectivity. This finding indicates that based on the simulation results, the diffusivity is an important design parameter for the future improvement of dual layer ammonia oxidation catalysts. The development of SCR washcoats with higher diffusivities would allow an increase in the catalyst's NH_3 conversion without a loss in product selectivity.

With the demonstrated high impact of the SCR layer's diffusion coefficients on the NH_3 conversion, it is clear that the agreement between the experimental and computed NH_3 conversion shown in Fig. 5 can only be obtained with a very good value for the diffusion coefficient. It might seem that the agreement between experiment and model predictions was better than what could be expected based on the uncertainty in the a priori estimation of the diffusion coefficient (see Section 2.2.5). This finding would mean that our choice of the diffusion coefficient would at least partially have to be considered as a lucky guess. However, the sensitivity study presented in Fig. 7 suggests that if the diffusion coefficient of the upper layer is regarded as an additional adjustable parameter, this parameter could be determined with a high degree of accuracy from a single experiment with a dual layer catalyst. The model could then be used for further design studies in the same way as demonstrated in this paper.

3.5.3. Variation of catalyst size

One important design parameter for the ammonia slip catalyst is catalyst size, especially because the ammonia slip catalyst is frequently coated as a short zone on the rear side of the SCR catalyst and therefore reduces the volume of the SCR catalyst. In the previous sections, the catalyst was studied at a relatively high space

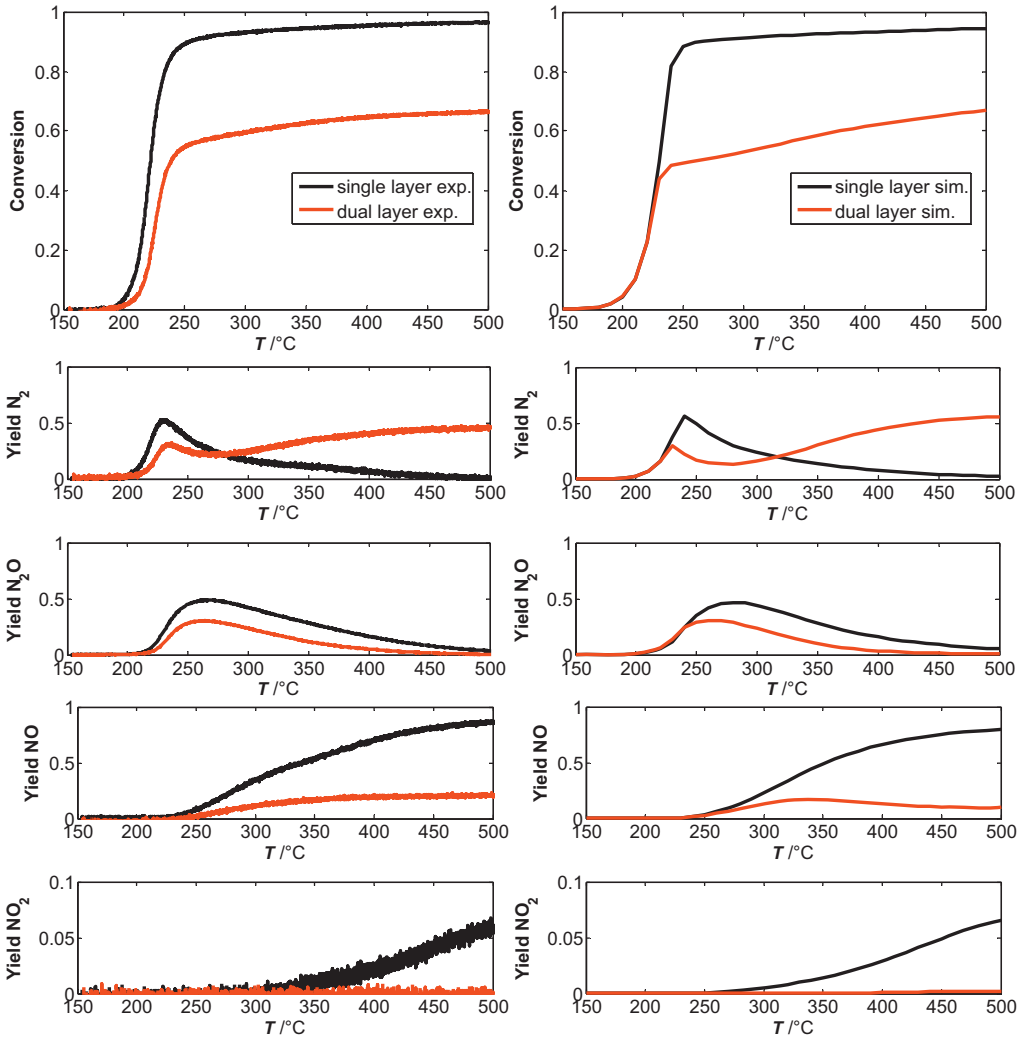

Fig. 5. Comparison of single and dual layer performance for experiments and simulation: conversion of ammonia and yields of products are plotted vs. temperature. On the left side, the experiments are shown, and on the right side, simulation results are shown for the Pt single layer and dual layer catalyst (300 ppm NH_3, 6% O_2, 5% H_2O (in the experiment), GHSV: 300,000 h^{-1}).

velocity of 300,000 h^{-1}. In this section, we studied the effect of catalyst size on conversion and selectivity.

For the study presented in this section, we define an arbitrary target NH_3 conversion of 85% at 450 °C. At the original catalyst size (space velocity 300,000^{-1}), this conversion target required a relatively thin SCR layer of 22 μm (compare Fig. 8). In a next step, the volume of the catalyst was increased by a factor of two, resulting in a space velocity of 150,000 h^{-1}. In this step, the thicknesses of both layers and the overall platinum loading in the catalyst were kept constant. The increased catalyst size leads to simultaneous improvements in NH_3 conversion and selectivity. In a third step, the thickness of the SCR layer for the catalyst of step 2 was increased to 78 μm, which resulted in our target conversion of 85%. The increase in SCR washcoat thickness leads to a further improvement in N_2 selectivity.

The study presented in this section shows that for a given target conversion, the optimal thickness of the SCR layer depends on the catalyst size. Such interrelations between different design parameters are easily overlooked in a purely experimental development process. It is one of the strengths of a simulation-supported development approach that such interrelations can be discovered early in the process and can then be taken into account in the design of the experimental program.

3.5.4. *The influence of NO oxidation in the Pt layer on the performance of the dual layer catalyst*

Finally, we studied the influence of NO oxidation capacity of the platinum layer on the selectivity of the dual layer catalyst. The formation of NO_2 in the lower layer could potentially increase the NO_x conversion in the upper layer due to the fast SCR reaction.

A sensitivity analysis of our reaction mechanism revealed that under reaction conditions relevant for the dual layer catalyst, the rate determining step for NO oxidation is the surface reaction of NO with O (reaction (R11)). For the platinum-only single layer catalyst and the reaction conditions of Fig. 5, a variation of k_0 for reaction (R11) by factors of 0, 1, 4, 16 resulted in NO_2 yields at 346 °C of 0%, 1.4%, 5.0%, 15.0%.

Fig. 9 shows results for the dual layer catalyst while applying the same variation in the pre-exponential factor of reaction (R11). An initial observation from Fig. 9 is that in our model, a complete removal of the NO oxidation pathway ($k_0 = 0$) does not lead to a significant change in NO selectivity. Thus, in the current model, the NO_2 pathway does not play a significant role. Fig. 9 also shows that some improvement in the catalyst's N_2 selectivity could be obtained if one could increase the NO oxidation capacity of the platinum layer by a factor of 8 or even 16.

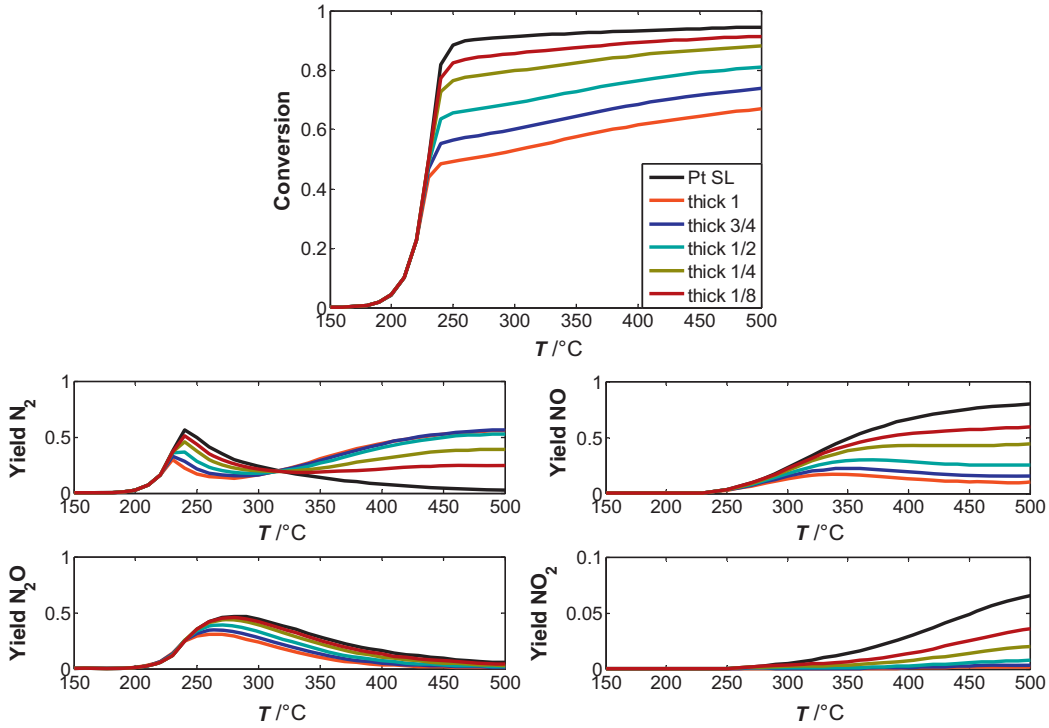

Fig. 6. Influence of the SCR washcoat loading on the performance of the dual layer catalyst: conversion of NH_3 and yield of products are plotted vs. temperature for different thicknesses of the SCR layer. A nominal thickness of 1 corresponds to washcoat thickness of 71 μm (300 ppm NH_3, 6% O_2, GHSV 300,000 h^{-1}).

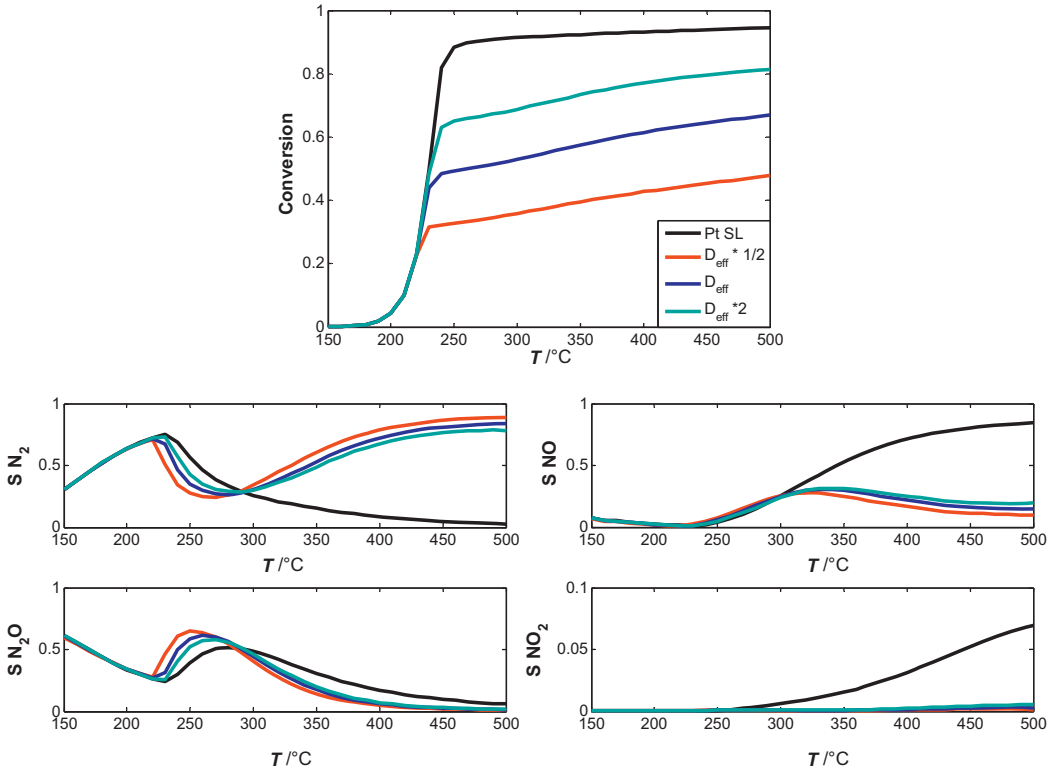

Fig. 7. Influence of the diffusion coefficient in the SCR layer on the performance of the dual layer catalyst: conversion of NH_3 and selectivity to products are plotted vs. temperature. The diffusion coefficient in the Pt layer was held constant. The simulation conditions were 300 ppm NH_3, 6% O_2 and GHSV 300,000 h^{-1}.

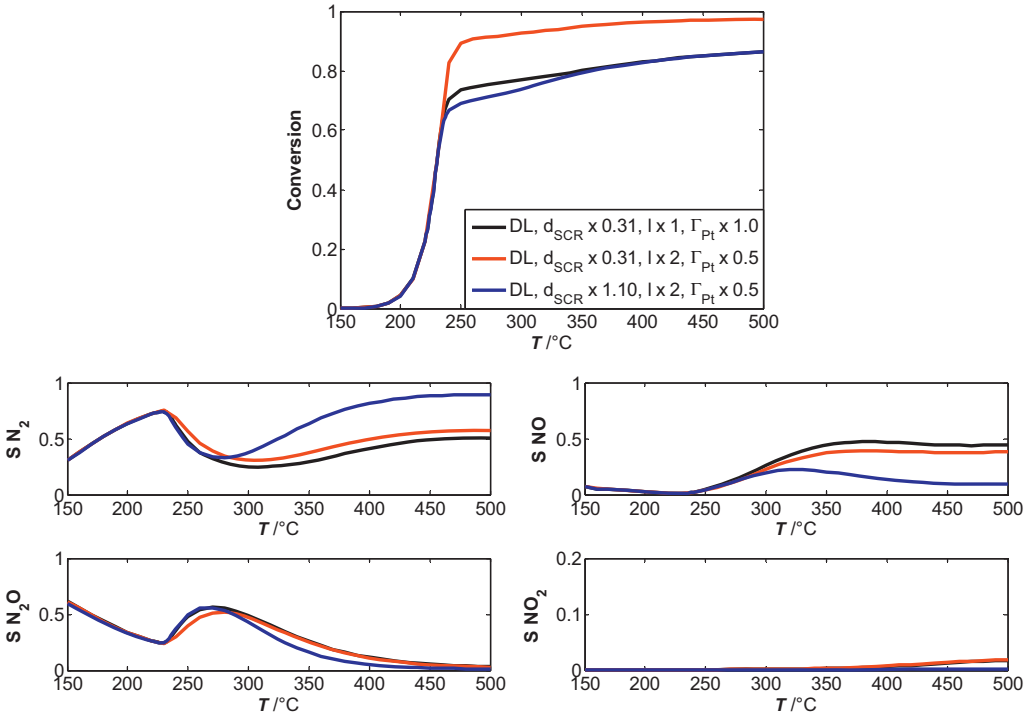

Fig. 8. An optimisation of the thickness of the SCR layer is shown for an arbitrary conversion target of 85% at 450 °C: the black curves show a catalyst operated at 300,000 h^{-1} SV with a layer thickness of 22 μm. The red curves show the results for a catalyst with the same SCR layer thickness but twice the length (half SV) and the same total Pt catalyst loading (half site concentration). The blue curve shows results for the same catalyst as the red curve, but with an optimised SCR layer thickness of 78 μm (300 ppm NH_3, 6% O_2). (For interpretation of the references to color in this figure legend, the reader is referred to the web version of this article.)

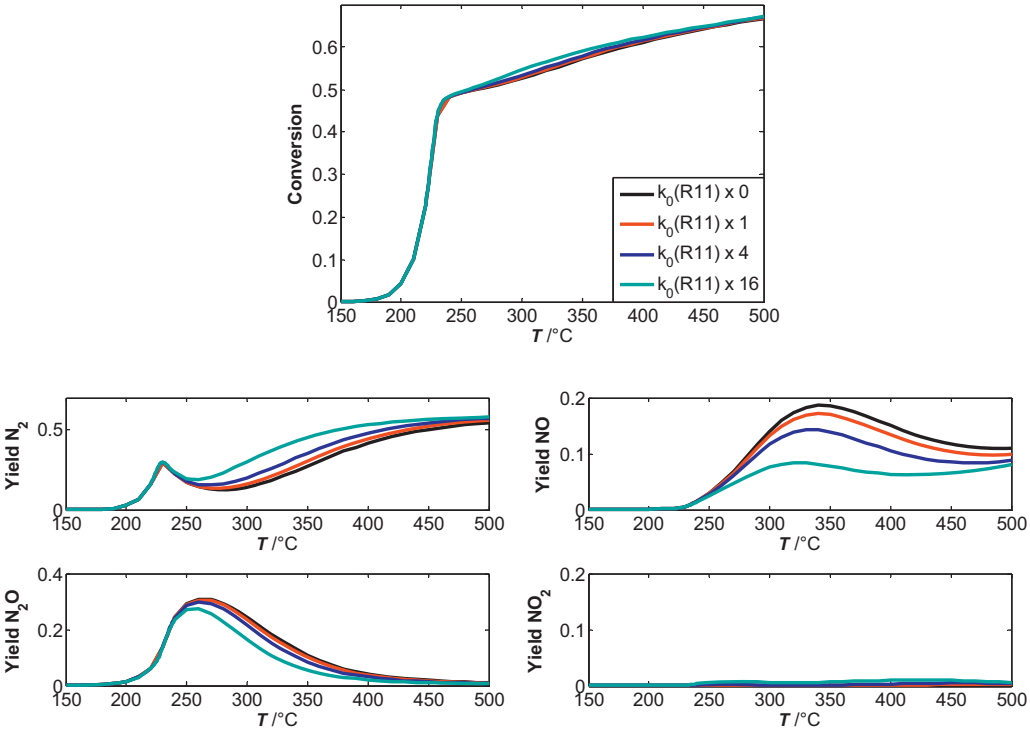

Fig. 9. The influence of NO oxidation in the Pt layer on the performance of the dual layer catalyst: the conversion of ammonia and the yield of products are plotted against temperature (300 ppm NH_3, 6% O_2, GHSV 300,000 h^{-1}).

4. Conclusion

We utilized experiments and computer simulations to compare the performance of a conventional single layer Pt/Al_2O_3 ammonia oxidation catalyst to the performance of a bifunctional catalyst with an additional SCR layer on top of a platinum layer.

The individual contributions and conclusions of the paper can be summarised as follows:

- A mechanistically based kinetic model for NH_3 oxidation under automotive conditions is presented. The model was parameterised based on laboratory data for a single layer Pt/Al_2O_3 catalyst and accurately described the reaction of NH_3 with O_2 and NO and their selectivities for N_2, N_2O and NO. Additionally, the oxidation of NO to NO_2 is included in the model.
- It is demonstrated in laboratory experiments that the dual layer catalyst shows reduced NO formation and improved selectivity for the desired product, N_2. However, a lower overall NH_3 conversion was observed for the dual layer catalyst.
- A 2-D model of one channel of a dual catalyst model was constructed. We show that the kinetic models could be efficiently implemented in a commercial simulation code using a spline interpolation of pre-computed source terms. Application of the spline interpolation leads to a speed up by a factor of 60 compared to a numerical solution of the rate equations.
- The experimental results for the dual layer catalyst were almost quantitatively reproduced by the model with the kinetics of the individual layers parameterised in separate experiments and no additional adjustable parameters for the dual layer model.

Compared to the conventional single layer catalyst, the design of layered multifunctional catalyst architectures involves an increased number of design parameters. In this article we show that numerical models can accurately predict the performance of such multilayer catalysts, and therefore, computer simulation can be used as tool for the design of such systems. The relevance of this work is not restricted to the design of ammonia oxidation catalysts. Already, most three-way catalysts use a dual layer design. Furthermore, dual layer multifunctional designs hold promise for other types of catalysts in the automotive and other fields. It is expected that simulation-based parameter studies such as the one demonstrated in this paper will help to facilitate the development of new multifunctional catalyst designs.

References

[1] N. Soeger, W. Schneider, Y. Demel, L. Mussmann, R. Sesselmann, T. Kreuzer, Patent WO200713767 (A1) (2007).
[2] M. Baerns, R. Imbihl, V.A. Kondratenko, R. Kraehnert, W.K. Offermans, R.A. van Santen, A. Scheibe, J. Catal. 232 (2005) 226–238.
[3] R. Imbihl, A. Scheibe, Y.F. Zeng, S. Günther, R. Kraehnert, V.A. Kondratenko, M. Baerns, W.K. Offermans, A.P.J. Jansen, R.A. van Santen, Phys. Chem. Chem. Phys. 9 (2007) 3522–3540.
[4] R. Kraehnert, M. Baerns, Chem. Eng. J. 137 (2008) 361–375.
[5] G. Novell-Leruth, J.M. Ricart, J. Perez-Ramirez, J. Phys. Chem. C 112 (2008) 13554–13562.
[6] W.K. Offermans, A.P.J. Jansen, R.A. van Santen, Surf. Sci. 600 (2006) 1714–1734.
[7] E.V. Rebrov, M.H.J.M. de Croon, J.C. Schouten, Inst. Chem. Eng. 81 (2003) 744–752.
[8] A. Scheibe, M. Hinz, R. Imbihl, Surf. Sci. 576 (2005) 131–144.
[9] A. Scheuer, M. Votsmeier, A. Schuler, J. Gieshoff, A. Drochner, H. Vogel, Top. Catal. 52 (2009) 1847–1851.
[10] P.S. Metkar, M.P. Harold, V. Balakotaiah, Appl. Catal. B (2010), doi:10.1016/j.apcatb.2011.09.019.
[11] G.C. Koltsakis, O. Haralampous, I. Koutoufaris, SAE Tech. Pap. (2010), 2010-01-0892.
[12] M. Votsmeier, Chem. Eng. Sci. 64 (2009) 1384–1389.
[13] M. Votsmeier, A. Scheuer, A. Drochner, H. Vogel, J. Gieshoff, Catal. Today 151 (2010) 271–277.
[14] D. Chatterjee, T. Burkhardt, M. Weibel, I. Nova, A. Grossale, E. Tronconi, SAE Tech. Pap. (2007), 2007-01-1136.
[15] D. Chatterjee, P. Kočí, V. Schmeißer, M. Marek, M. Weibel, B. Krutsch, Catal. Today 151 (2010) 395–409.
[16] S. Malmberg, M. Votsmeier, J. Gieshoff, N. Söger, L. Mussmann, A. Schuler, A. Drochner, Top. Catal. 42–43 (2007) 33–36.
[17] P. Markatou, J. Dai, A. Johansson, K. Wassim, M. Castagnola, T.C. Watling, M. Tutuianu, SAE Tech. Pap. (2011), 2011-01-1304.
[18] A. Schuler, M. Votsmeier, P. Kiwic, J. Gieshoff, W. Hauptmann, A. Drochner, H. Vogel, Chem. Eng. J. 154 (2009) 333–340.
[19] H. Sjövall, R.J. Blint, A. Gopinath, L. Olsson, Ind. Eng. Chem. Res. 49 (2010) 39–52.
[20] T.J. Wang, S.W. Bae, H.J. Kwon, Y.J. Kim, I.-S. Nam, M. Cha, G.K. Yeo, Ind. Eng. Chem. Res. 50 (2011) 2850–2864.
[21] P.S. Metkar, N. Salazar, R. Muncrief, V. Balakotaiah, M.P. Harold, Appl. Catal. B: Environ. 104 (2011) 110–126.
[22] M. Colombo, I. Nova, E. Tronconi, V. Schmeißer, B. Bandl-Konrad, L. Zimmermann, Appl. Catal. B (2010), doi:10.1016/j.apcatb.2011.09.023.
[23] W. Hauptmann, M. Votsmeier, H. Vogel, D.G. Vlachos, Appl. Catal. 397 (2011) 174–182.
[24] K.E. Brenan, S.L. Campbell, L.R. Petzold, Numerical solution of initial-value problems in differential-algebraic equations, Elsevier Science Publishing Co, New York, 1989.
[25] C. de Boor, A Practical Guide to Splines, Springer, New York, 1978.
[26] A. Scheuer, O. Hirsch, R. Hayes, H. Vogel, M. Votsmeier, Catal. Today 175 (2011) 141–146.
[27] R.E. Hayes, B. Liu, R. Moxom, M. Votsmeier, Chem. Eng. Sci. 59 (2004) 3169–3181.
[28] E.N. Fuller, P.D. Schettler, J.C. Giddings, Ind. Eng. Chem. 58 (1966) 18–27.
[29] P. Kočí, F. Štěpánek, M. Kubíček, M. Marek, Mol. Simul. 33 (2007) 369–377.
[30] I. Nova, D. Bounechada, R. Maestri, E. Tronconi, A. Heibel, T.A. Collins, T. Boger, Ind. Eng. Chem. Res. 50 (2011) 299–309.
[31] F. Zhang, R.E. Hayes, S.T. Kolaczkowski, Chem. Eng. Res. Des. 82 (2004) 481–489.
[32] W. Hauptmann, M. Votsmeier, J. Gieshoff, A. Drochner, H. Vogel, Appl. Catal. B 93 (2009) 22–29.
[33] A.B. Mhadeshwar, H. Wang, D.G. Vlachos, J. Phys. Chem. B 107 (2003) 12721–12733.
[34] O. Deutschmann, Computational fluid dynamics simulation of catalytic reactors, in: G. Ertl, H. Knözinger, F. Schütz, J. Weitkamp (Eds.), Handbook of Heterogeneous Catalysis, Wiley-VCH, Weinheim, 2008.
[35] A. Scheuer, A. Drochner, J. Gieshoff, H. Vogel, M. Votsmeier, Catal. Today, submitted for publication.